Electronic Supplementary Material (ESI) for Journal of Materials Chemistry A.
This journal is © The Royal Society of Chemistry 2022

Electronic Supplementary Material (ESI) for Journal of Materials Chemistry A.

Supporting Information

Adjustable Antiperovskite Cobalt-Based Nitrides as Efficient Electrocatalysts for Overall Water Splitting

Lili Zhu,[ab] Changdian Li,[ab] Han Li,[ab] Hui Li,[ab] Ziqiang Wu,[ab] Yanan Huang,[*a] Xuebin Zhu[*ab] and Yuping Sun [acd]

[a] Key Laboratory of Materials Physics, Institute of Solid State Physics, HFIPS，Chinese Academy of Sciences, Hefei 230031, People's Republic of China

[b] University of Science and Technology of China, Hefei 230026, People's Republic of China

[c] High Magnetic Field Laboratory, HFIPS, Chinese Academy of Sciences, Hefei 230031, People's Republic of China

[d] Collaborative Innovation Center of Advanced Microstructures, Nanjing University, Nanjing 210093, People's Republic of China

***Corresponding authors E-mail:** ynhuang@issp.ac.cn; xbzhu@issp.ac.cn

List of Texts, Figures and Tables

Text S1. Experimental section.

Text S2. Material characterizations.

Text S3. Electrochemical measurements and evaluations.

Fig. S1 (a) XRD pattern and (b) SEM image of bare nickel foam (NF).

Fig. S2 XRD patterns of $CoN_{0.73}Co_3$.

Fig. S3 XPS spectra of $CoN_{0.73}Co_3$, (a) survey scan, (b) Co 2*p*, (c) N 1*s*.

Fig. S4 (a, b) SEM images of Cu-Co bimetallic hydroxide/NF (precursor of $CuNCo_3$/NF). (c) XRD patterns of Cu-Co bimetallic hydroxide/NF. (d, e) SEM images of Co hydroxide/NF (precursor of $CoN_{0.73}Co_3$/NF). (f) XRD patterns of Co hydroxide/NF.

Fig. S5 Electrocatalytical OER testing in 1 M KOH. (a) LSV curves for precursors of $CuNCo_3$/NF, $CoN_{0.73}Co_3$/NF, RuO_2 and NF. (b) Tafel plots. (c) Nyquist plots and equivalent circuit.

Fig. S6 CV curves of OER testing for (a) $CuNCo_3$/NF and (b) $CoN_{0.73}Co_3$/NF with 20, 40, 60, 80 and 100 mV s^{-1} in non-Faradaic potential range.

Fig. S7 CV curves of OER testing for precursors of (a) $CuNCo_3$/NF and (b) $CoN_{0.73}Co_3$/NF with 20, 40, 60, 80 and 100 mV s^{-1} in non-Faradaic potential range.

Fig. S8 Electrocatalytical HER testing results in 1 M KOH. (a) LSV curves for precursors of $CuNCo_3$/NF and $CoN_{0.73}Co_3$/NF, RuO_2 and NF. (b) Tafel plots. (c) Nyquist plots and equivalent circuit.

Fig. S9 (a) LSV curves and (b) Tafel plots with the mass activity of RuO_2, $CuNCo_3$/NF

and $CoN_{0.73}Co_3$/NF for OER. (c) LSV curves and (d) Tafel plots with the mass activity of 20 wt% Pt/C, $CoN_{0.73}Co_3$/NF and $CuNCo_3$/NF for HER.

Fig. S10 (a) LSV curves and (b) Tafel plots with the mass activity for RuO_2, precursors of $CuNCo_3$/NF and $CoN_{0.73}Co_3$/NF for OER. (c) LSV curves and (d) Tafel plots with the mass activity for 20 wt% Pt/C, precursors of $CoN_{0.73}Co_3$/NF and $CuNCo_3$/NF for HER.

Fig. S11 Polarization curves of (a) OER, (b) HER and (c) two-electrode system for overall water splitting with maximum current density of 400 mA cm^{-2}.

Fig. S12 (a) LSV curves of two-electrode electrolyzers ($CuNCo_3$/NF || $CoN_{0.73}Co_3$/NF and RuO_2/NF || 20 wt% Pt/C/NF). (b) Stability test of two-electrode electrolyzer (RuO_2/NF || 20 wt% Pt/C/NF).

Fig. S13 The long-term durability test of $CuNCo_3$/NF || $CoN_{0.73}Co_3$/NF at a current density of 100 mA cm^{-2}.

Fig. S14 Stability tests for (a) OER of $CuNCo_3$/NF and (b) HER of $CoN_{0.73}Co_3$/NF.

Fig. S15 XRD patterns of (a) $CuNCo_3$/NF, (b) $CoN_{0.73}Co_3$/NF electrodes after stability test (48 h).

Fig. S16 The high-resolution XPS results for Co 2*p*, Cu 2*p*, N 1*s* and O 1*s* of $CuNCo_3$/NF electrode with initial and after stability test (48 h).

Fig. S17 The high-resolution XPS results for Co 2*p* and N 1*s* of $CoN_{0.73}Co_3$/NF electrode with initial and after stability test (48 h).

Fig. S18 The TEM mapping of $CuNCo_3$ after stability test (48 h).

Fig. S19 The TEM mapping of $CoN_{0.73}Co_3$ after stability test (48 h).

Table S1. The comparison of various electrocatalysts for overall water splitting.

Table S2. The comparison of OER activity of the $CuNCo_3$/NF with that of other reported catalysts at the current density of 10 mA cm^{-2}.

Table S3. The comparison of HER activity of the $CoN_{0.73}Co_3$/NF with that of other reported catalysts at the current density of 10 mA cm^{-2}.

Text S1. Experimental section

Preparation of $CuNCo_3$/NF and $CoN_{0.73}Co_3$/NF: In processing, 1 mmol $Cu(NO_3)_2{\cdot}3H_2O$ (99.0%, Sinophorm Chemical Reagent Co., Ltd), 3 mmol $Co(NO_3)_2{\cdot}6H_2O$ (98.5% Sinophorm Chemical Reagent Co., Ltd) and 14 mmol $Co(NH_2)_2$ (99.0% Sinophorm Chemical Reagent Co., Ltd) were dissolved into 60 mL deionized water and stirred. Then, the prepared aqueous solution and a NF substrate (XRD pattern and SEM images of bare NF were displayed in Fig. S1) were transferred into a 100 mL stainless-steel autoclave and reacted at 120°C for 10h. After the reaction, the sample was washed with deionized water and alcohol, and dried in an oven at 60°C. The obtained hydrothermal precursor was Cu-Co bimetallic hydroxide/NF. Then, the hydrothermal precursor of Cu-Co bimetallic hydroxide/NF was annealed at 420 °C under the flowing NH_3 atmosphere for 2h (as depicted in Scheme 1). The obtained product was $CuNCo_3$/NF. The catalyst loading mass of $CuNCo_3$/NF is ~4 mg cm^{-2}. Similar processing was carried out to prepare the $CoN_{0.73}Co_3$/NF, in which 4 mmol $Co(NO_3)_2{\cdot}6H_2O$ was used to prepare the aqueous solution without addition of $Cu(NO_3)_2{\cdot}3H_2O$. The obtained product was $CuNCo_3$/NF. The catalyst loading mass of

$CuNCo_3$/NF is ~4 mg cm^{-2}.

Preparation of Pt/C electrode and RuO_2 electrode: The 20 wt% Pt/C and RuO_2 were used as the reference samples for HER and OER, respectively. 10 mg catalyst was dispersed into the solution with 950 μL isopropanol and 50 μL 5 wt% Nafion, and ultrasonically stirred for more than 40 minutes until the dispersed ink was obtained. Then, 400 μL of the dispersed ink was loaded onto NF with the size of 1×1 cm^2 (loading mass of 4 mg cm^{-2}). Finally, the as-prepared electrode was dried at room temperature for electrochemical measurements.

Text S2. Material characterizations

X-ray diffraction (XRD, Philips X′pert PRO). Scanning electron microscope (SEM, Quanta 200FEG). Transmission electron microscope (TEM, JEM-2100). The X-ray photoelectron spectroscopy (XPS, Thermo Scientific K-Alpha device with excitation source of Al K_α).

Text S3. Electrochemical measurements and evaluations

The conventional three-electrode system equipped with N_2 gas flow system was utilized for electrochemical measurements at room temperature in 1 M KOH electrolyte on a CHI660E workstation. Hg/HgO and graphite rod were used as the reference electrode and counter electrode, respectively. The prepared samples were used as the working electrodes. All the potentials were calibrated to reversible hydrogen electrode (RHE) according to the equation E (*vs.* RHE) = E (*vs.* Hg/HgO) + $E^{o}_{Hg/HgO}$ + 0.0591 pH ($E^{o}_{Hg/HgO}$: 0.098V, pH: 14). LSV was measured at a scan rate of 2 mV s^{-1}. A series of

CV measurements were performed at different scan rates within 20 - 100 mV s^{-1} in the range of 1.025 - 1.125 V (*vs.* RHE) in order to calculate the ECSA. The ECSA was calculated as ECSA=C_{dl}/C_s. C_{dl} is double-layer capacitance and C_s represents 40 μF cm^{-2} in 1 M KOH. The C_{dl} was obtained by fitting the half slope of current density and scanning rate at the average potential range of CV. EIS was obtained at overpotential of 300 mV and -200 mV (*vs.* RHE) for OER and HER respectively in the frequency range of 0.1 - 10^5 Hz with 5 mV amplitude. The stability of the catalyst was tested by chronoamperometry. All data were calibrated by 90 % iR compensation.

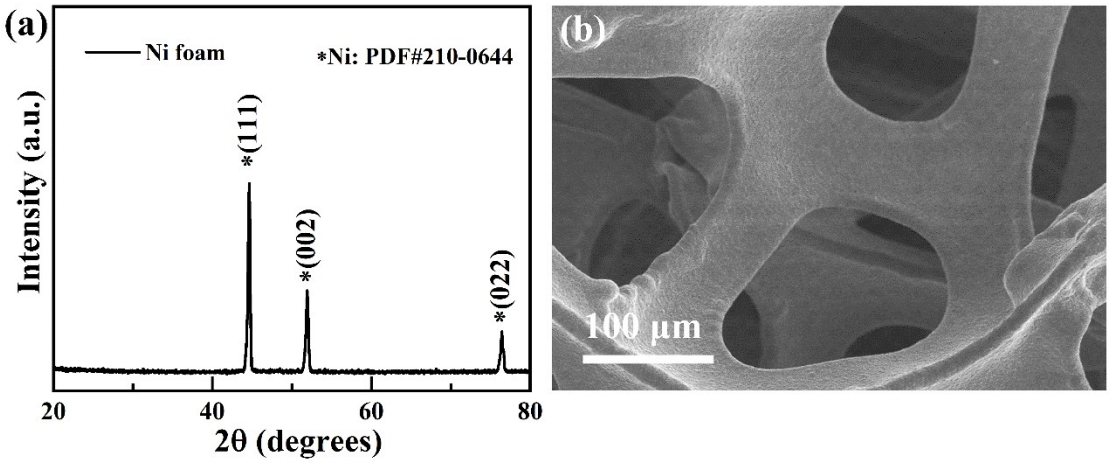

Fig. S1 (a) XRD pattern and (b) SEM image of bare nickel foam (NF).

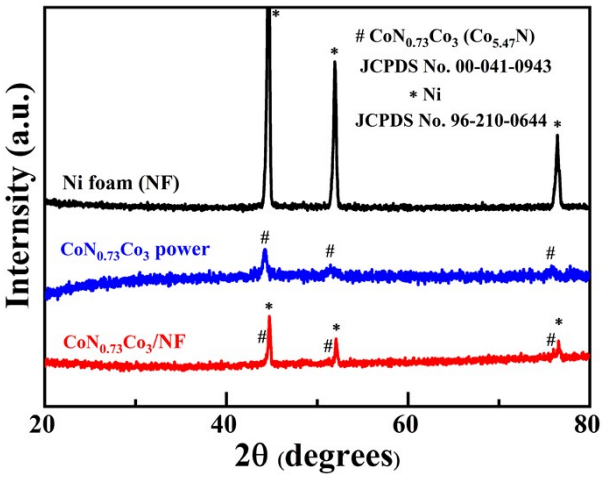

Fig. S2 XRD patterns of $CoN_{0.73}Co_3$.

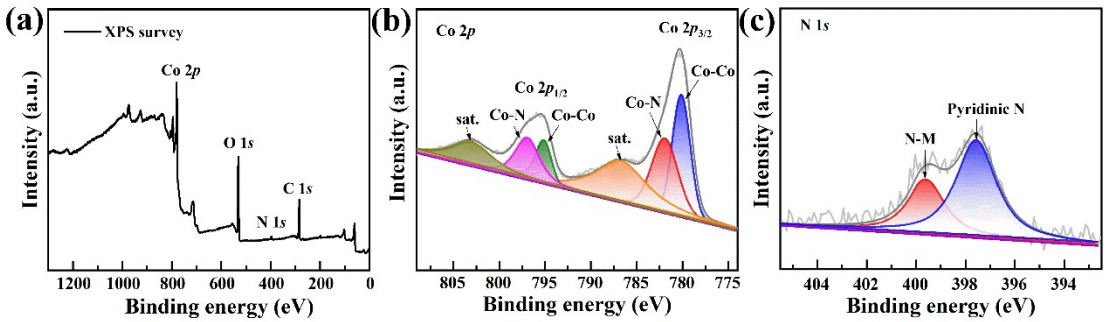

Fig. S3 XPS spectra of $CoN_{0.73}Co_3$, (a) survey scan, (b) Co 2*p*, (c) N 1*s*.

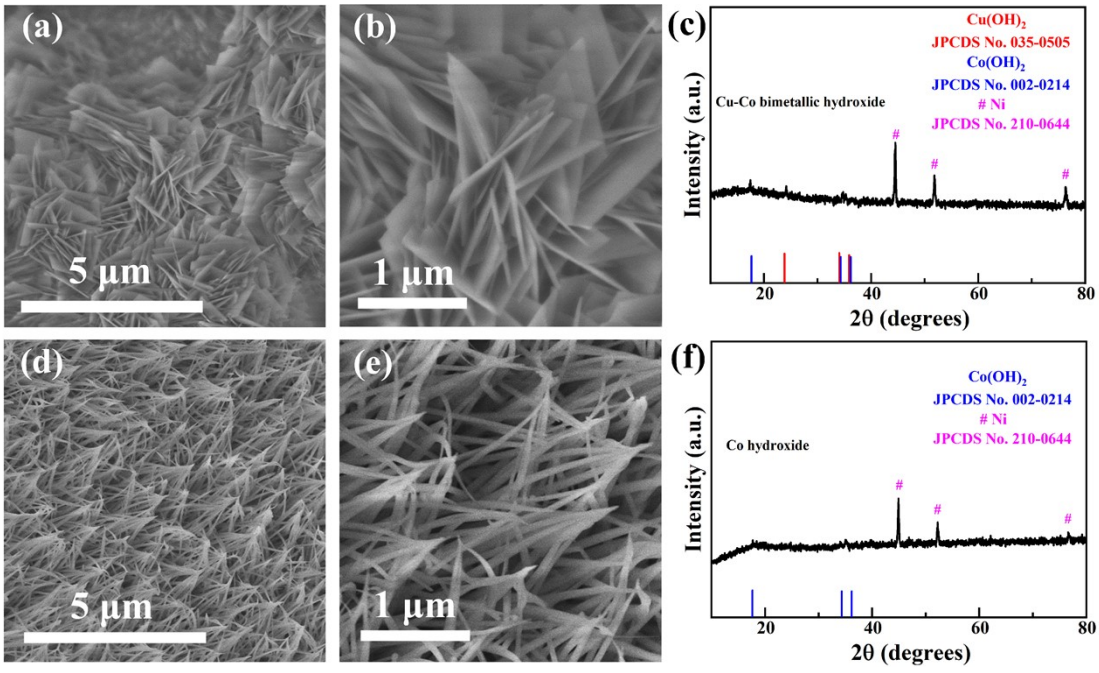

Fig. S4 (a, b) SEM images of Cu-Co bimetallic hydroxide/NF (precursor of $CuNCo_3$/NF). (c) XRD patterns of Cu-Co bimetallic hydroxide/NF. (d, e) SEM images of Co hydroxide/NF (precursor of $CoN_{0.73}Co_3$/NF). (f) XRD patterns of Co hydroxide/NF.

In Fig. S4c, XRD patterns of as-prepared Cu-Co bimetallic hydroxide/NF (precursor of $CuNCo_3$/NF) presents the coexistence of $Cu(OH)_2$ (JPCDS No.035-0505), $Co(OH)_2$ (JPCDS No. 002-0214) and NF (JPCDS No. 210-0644) phases. The peaks at 24.02°, 33.83° and 35.52°can be indexed to the (021), (002) and (111) plane of $Cu(OH)_2$, and additional peaks at 17.56°, 34.62° and 36.27° can be assigned to the $Co(OH)_2$.

In Fig. S4f, XRD patterns of as-prepared Co hydroxide/NF (precursor of $CoN_{0.73}Co_3$/NF) shows the coexistence of $Co(OH)_2$ (JPCDS No. 002-0214) and NF (JPCDS No. 210-0644) phases. The peaks at about 17.73°, 34.21° and 35.95° can be indexed to the $Co(OH)_2$.

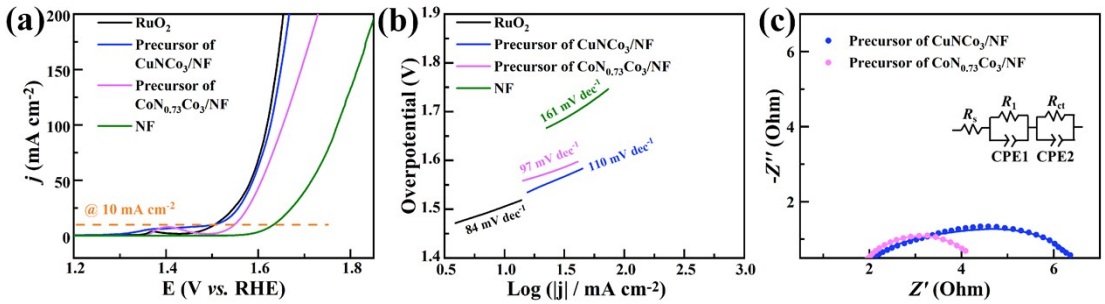

Fig. S5 Electrocatalytical OER testing in 1.0 M KOH. (a) LSV curves for precursors of $CuNCo_3$/NF, $CoN_{0.73}Co_3$/NF, RuO_2 and NF. (b) Tafel plots. (c) Nyquist plots and equivalent circuit.

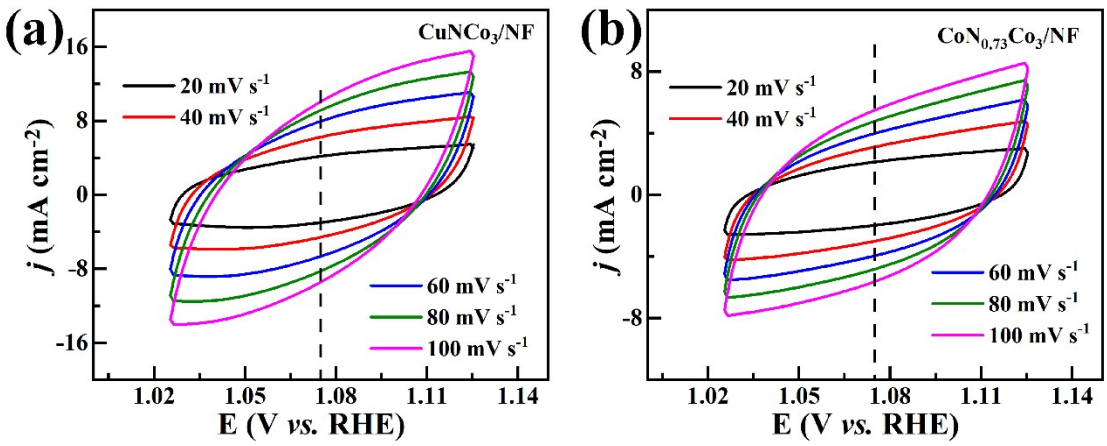

Fig. S6 CV curves of OER testing for (a) $CuNCo_3$/NF and (b) $CoN_{0.73}Co_3$/NF with 20, 40, 60, 80 and 100 mV s^{-1} in non-Faradaic potential range.

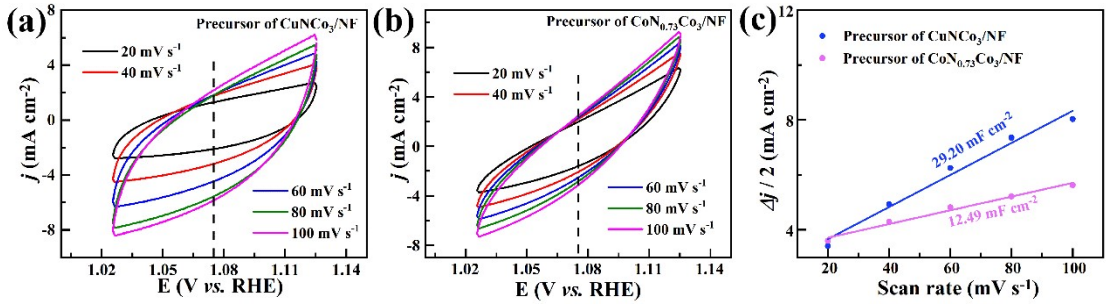

Fig. S7 CV curves of OER testing for precursors of (a) $CuNCo_3$/NF and (b) $CoN_{0.73}Co_3$/NF with 20, 40, 60, 80 and 100 mV s^{-1} in non-Faradaic potential range.

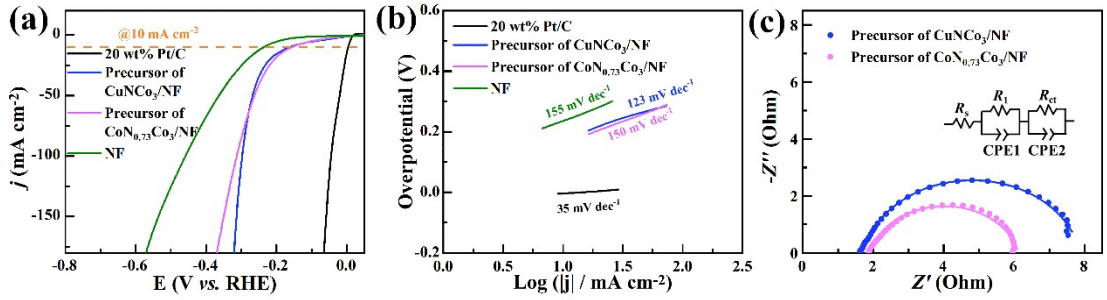

Fig. S8 Electrocatalytical HER testing results in 1 M KOH. (a) LSV curves for precursors of $CuNCo_3$/NF and $CoN_{0.73}Co_3$/NF, RuO_2 and NF. (b) Tafel plots. (c)

Nyquist plots and equivalent circuit.

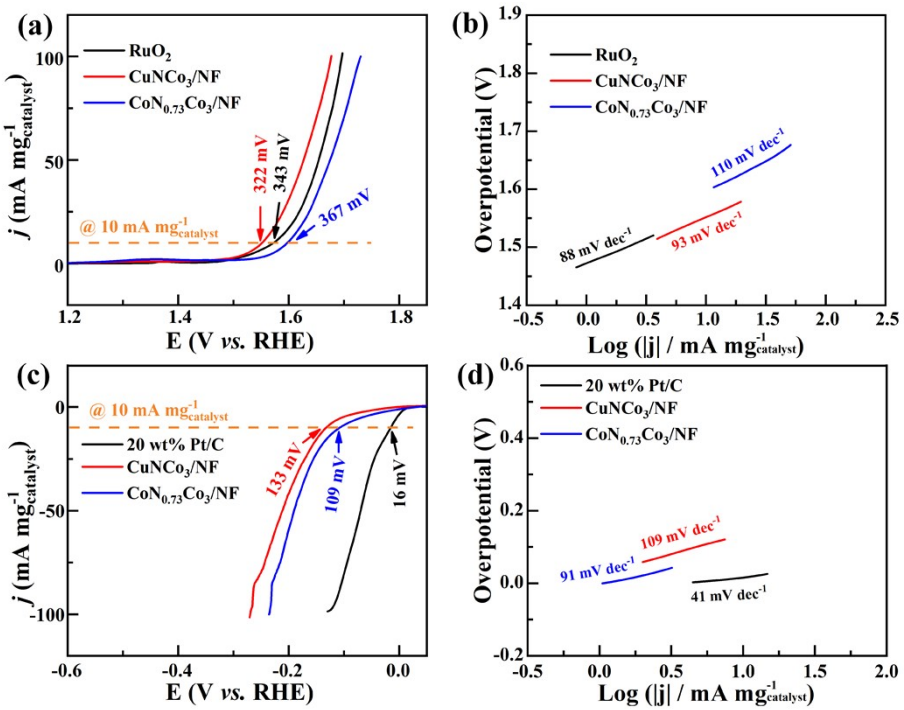

Fig. S9 (a) LSV curves and (b) Tafel plots with the mass activity of RuO_2, $CuNCo_3$/NF and $CoN_{0.73}Co_3$/NF for OER. (c) LSV curves and (d) Tafel plots with the mass activity of 20 wt% Pt/C, $CoN_{0.73}Co_3$/NF and $CuNCo_3$/NF for HER.

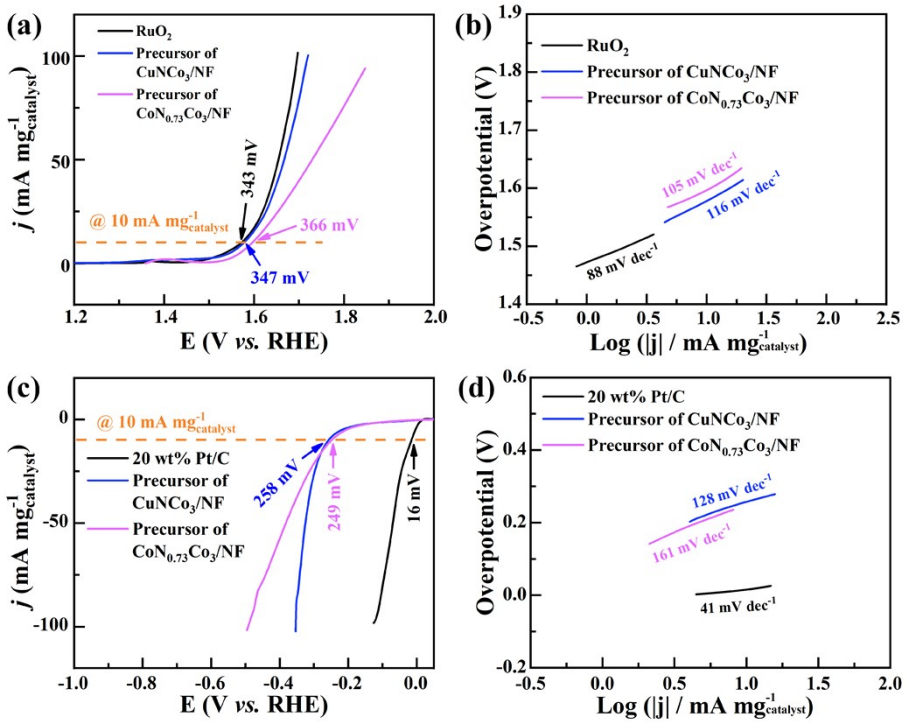

Fig. S10 (a) LSV curves and (b) Tafel plots with the mass activity for RuO_2, precursors of $CuNCo_3$/NF and $CoN_{0.73}Co_3$/NF for OER. (c) LSV curves and (d) Tafel plots with the mass activity for 20 wt% Pt/C, precursors of $CoN_{0.73}Co_3$/NF and $CuNCo_3$/NF for HER.

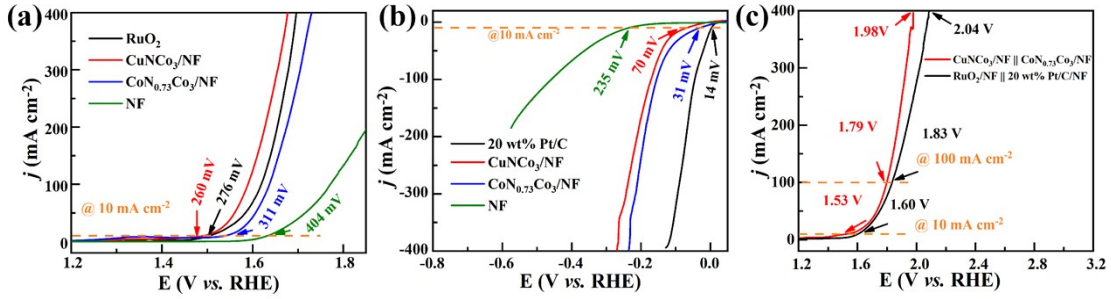

Fig. S11 Polarization curves of (a) OER, (b) HER and (c) two-electrode system for overall water splitting with maximum current density of 400 mA cm^{-2}.

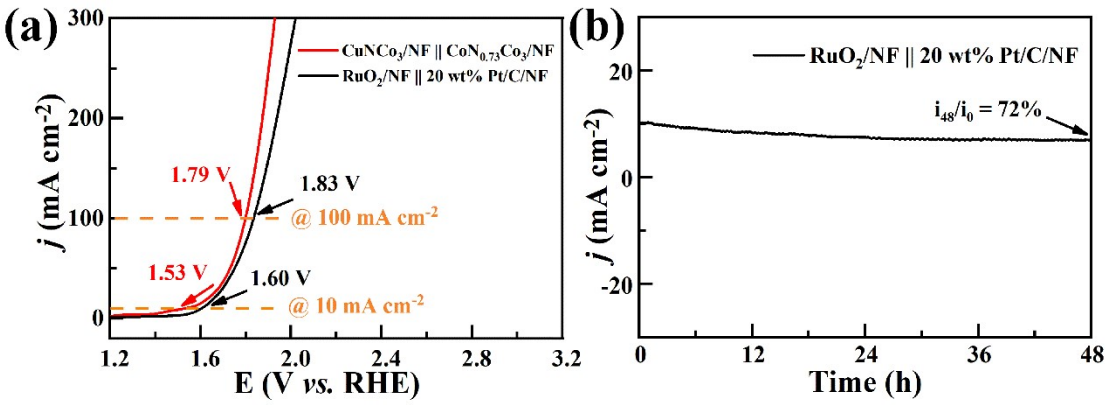

Fig. S12 (a) LSV curves of two-electrode electrolyzers ($CuNCo_3$/NF || $CoN_{0.73}Co_3$/NF and RuO_2/NF || 20 wt% Pt/C/NF). (b) Stability test of two-electrode electrolyzer (RuO_2/NF || 20 wt% Pt/C/NF).

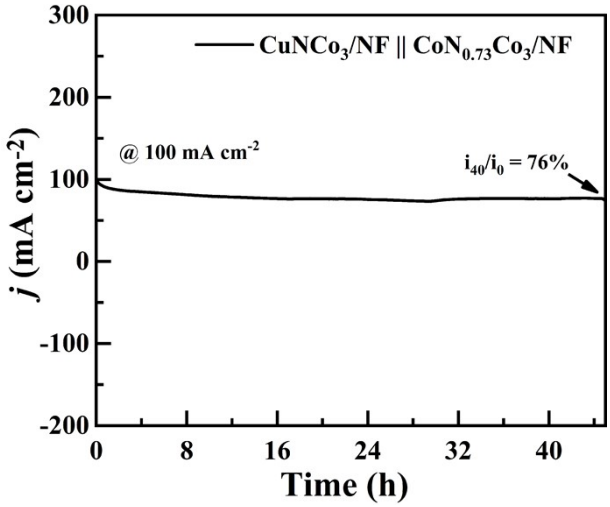

Fig. S13 The long-term durability test of $CuNCo_3$/NF || $CoN_{0.73}Co_3$/NF at a current density of 100 mA cm^{-2}.

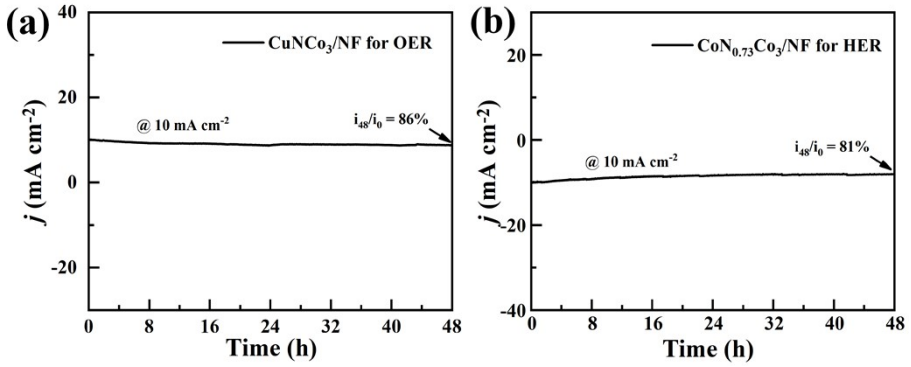

Fig. S14 Stability tests for (a) OER of $CuNCo_3$/NF and (b) HER of $CoN_{0.73}Co_3$/NF.

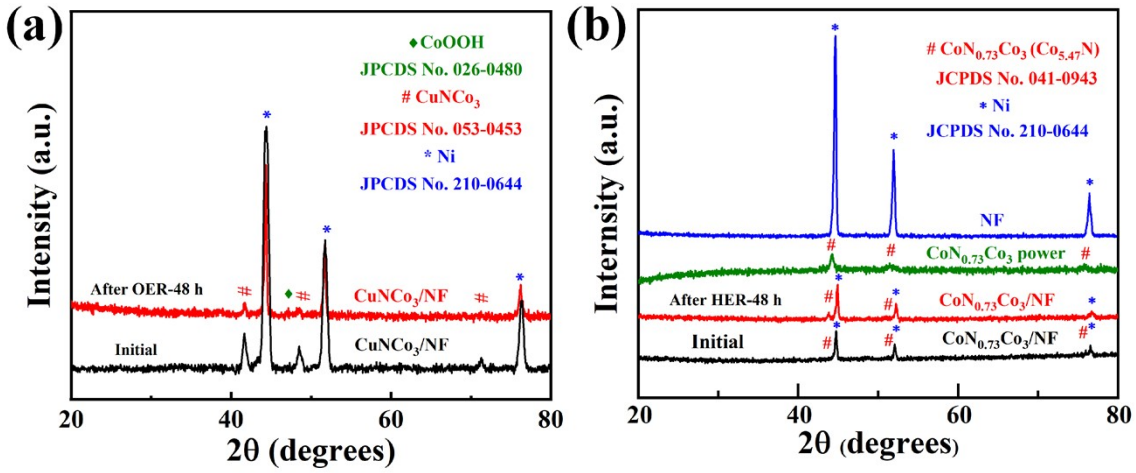

Fig. S15 XRD patterns of (a) $CuNCo_3$/NF, (b) $CoN_{0.73}Co_3$/NF electrodes after stability test (48 h).

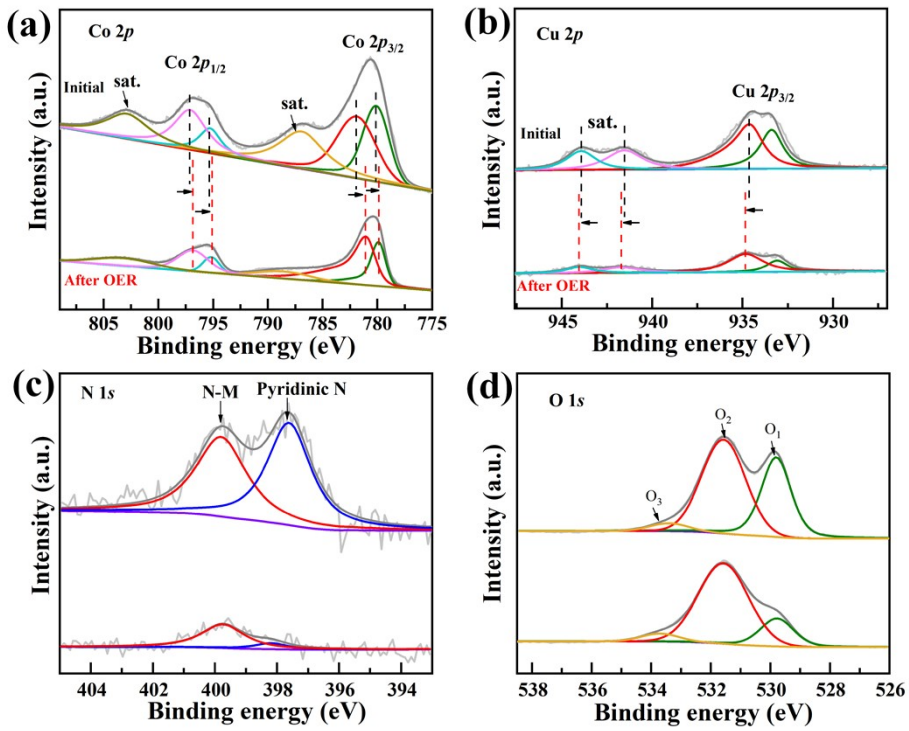

Fig. S16 The high-resolution XPS results for Co 2*p*, Cu 2*p*, N 1*s* and O 1*s* of $CuNCo_3$/NF electrode with initial and after stability test (48 h).

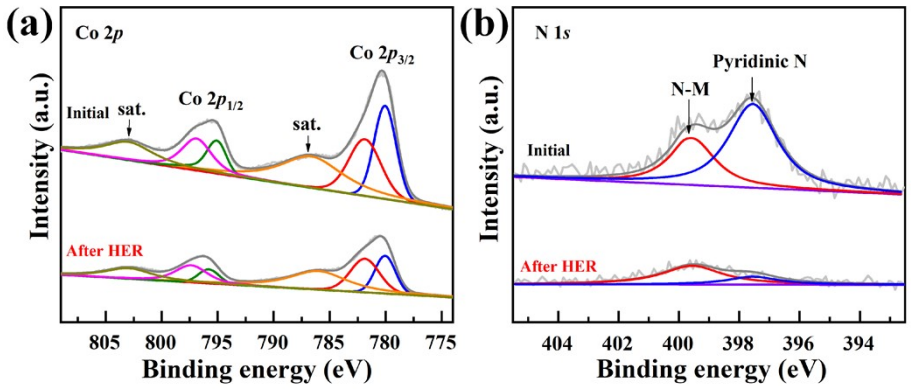

Fig. S17 The high-resolution XPS results for Co 2*p* and N 1*s* of $CoN_{0.73}Co_3$/NF electrode with initial and after stability test (48 h).

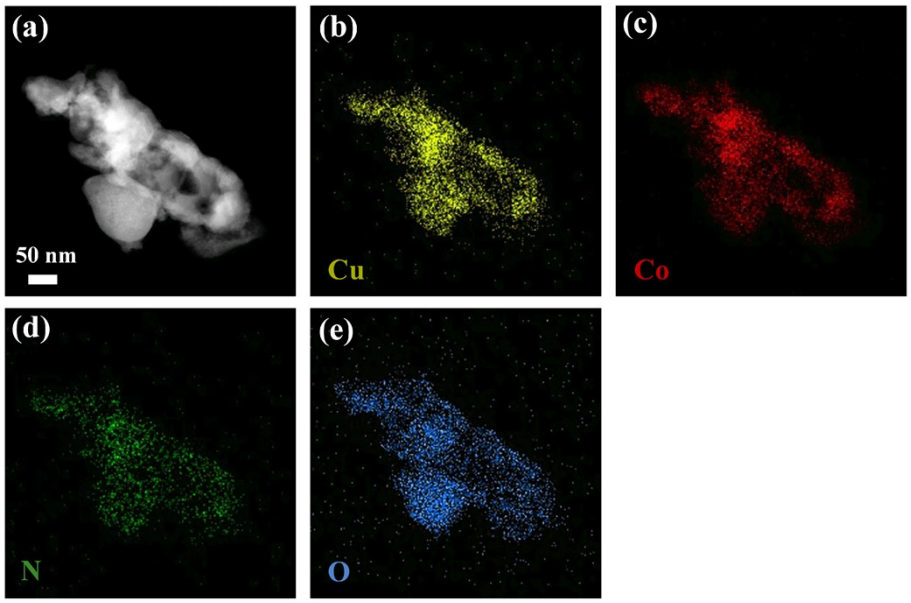

Fig. S18 The TEM mapping of $CuNCo_3$ after stability test (48 h).

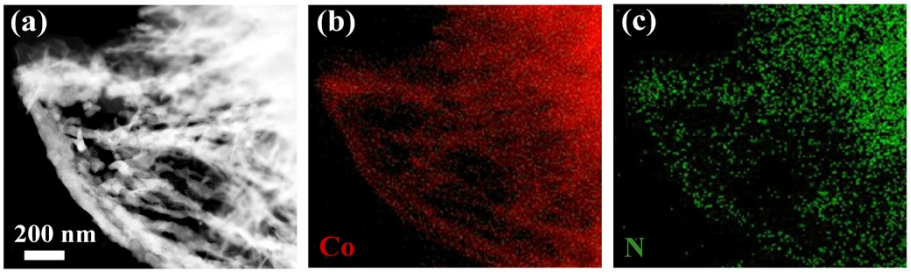

Fig. S19 The TEM mapping of $CoN_{0.73}Co_3$ after stability test (48 h).

The calculation of electrochemical surface area:

The electrochemical surface area (ECSA) of each catalyst can be calculated according to: $A_{ESCA} = {C_{dl}}/{\left(C_s \, per \, ESCA \, cm^2\right)}$

C_s is the specific capacitance of atomically smooth planar surface in respective electrolytic medium.[1] In this work, C_s was 40 μF cm^{-2} for 1.0 M KOH.[2]

Table S1. The comparison of various electrocatalysts for overall water splitting.

Electrocatalysts	Morphology	iR compensation	Voltage at 10 mA cm^{-2} (V)	References
$CuNCo_3$ || $CoN_{0.73}Co_3$	Nanosheets and Nanowires	With iR compensation	1.53	This work
$FeNi_3N$ || $FeNi_3N$	Nanoparticles	With iR compensation	1.62	3
V-$FeNi_3N/Ni_3N$ || V-$FeNi_3N/Ni_3N$	Nanoparticles	With iR compensation	1.63	4
TiN@Ni_3N || TiN@Ni_3N	Nanowires	With iR compensation	1.64	5
Ni_3FeN || Ni_3FeN	Nanosheets	With iR compensation	1.495	6
Co_3FeN_x || Co_3FeN_x	Nanowires	With iR compensation	1.539	7
NiCoP/rGO || NiCoP/rGO	Nanocrystals	Without iR compensation	1.59	8
$InNNi_3$/InNi (oxy)hydroxide || $InNNi_3$/InNi (oxy)hydroxide	Core-shell structure	Without iR compensation	1.64	9
$CoMoN_x$ || $CoMoN_x$	Nanosheets	With iR compensation	1.55	10
Fe_3N@Co_4N@CoFe || Fe_3N@Co_4N@CoFe	Nanoparticles	With iR compensation	1.59	11

Table S2. The comparison of OER activity of the $CuNCo_3$/NF with that of other reported catalysts at the current density of 10 mA cm^{-2}.

Electrocatalysts	η_{10} (mV *vs.* RHE)	Tafel slope (mV dec^{-1})	Electrolyte	References
$CuNCo_3$	260	87	1.0 M KOH	This work

$FeNi_3N$	222	~42	1.0 M KOH	[12]
HfN	358	85	1.0 M NaOH	[13]
$NiCo_2N$	289	46	1.0 M KOH	[14]
Fe_2Ni_2N/rGO	290	~41	0.1 M KOH	[15]
CoAl-Fe_2N/Fe_3N	307	69	1.0 M KOH	[16]
NiMoN-550	295	94	1.0 M KOH	[17]
Ni_3FeN	355	70	0.1 M KOH	[18]
$Ni_{0.65}Fe_{0.35}$@PCN	310	38	1.0 M KOH	[19]
NiCoNP	290	41	1.0 M KOH	[20]

Table S3. The comparison of HER activity of the $CoN_{0.73}Co_3$/NF with that of other reported catalysts at the current density of 10 mA cm^{-2}.

Electrocatalysts	η_{10} (mV *vs.* RHE)	Tafel slope (mV dec^{-1})	Electrolyte	References
$CoN_{0.73}Co_3$/NF	31	82	1.0 M KOH	This work
0.18 $Ag/Ag_{0.80}Ni_{0.20}NNi_3$	81	59	1.0 M KOH	[21]
$NiCo_2N$	48	~79	1.0 M KOH	[22]
Co_2Ni_1N	~103	~61	1.0 M KOH	[23]
Ni/C_3N_4	222	128	1.0 M NaOH	[24]
VN/WN@NC	122	67	1.0 M KOH	[25]
Ru-VN-2	144	73	1.0 M KOH	[26]
Nb_2N	~96	92	0.5 M H_2SO_4	[27]
Ni_3B-850	79	~85	0.5 M H_2SO_4	[28]

VCoN	179	123	1.0 M KOH	[29]

References

1 C. C. McCrory, S. Jung, I. M. Ferrer, S. M. Chatman, J. C. Peters and T. F. Jaramillo, *J. Am. Chem. Soc.*, 2015, **137**, 4347-4357.

2 C. C. McCrory, S. Jung, J. C. Peters and T. F. Jaramillo, *J. Am. Chem. Soc.*, 2013, **135**, 16977-16987.

3 B. Zhang, C. Xiao, S. Xie, J. Liang, X. Chen and Y. Tang, *Chem. Mater.*, 2016, **28**, 6934-6941.

4 J. Wang, Y. Sun, Y. Qi and C. Wang, *ACS Appl. Mater. Inter.*, 2021, **13**, 57392-57402.

5 Q. Zhang, Y. Wang, Y. Wang, A. M. Al-Enizi, A. A. Elzatahry and G. Zheng, *J. Mater. Chem. A*, 2016, **4**, 5713-5718.

6 Y. Wang, C. Xie, D. Liu, X. Huang, J. Huo and S. Wang, *ACS Appl. Mater. Inter.*, 2016, **8**, 18652-18657.

7 Y. Wang, D. Liu, Z. Liu, C. Xie, J. Huo and S. Wang, *Chem. Commun.*, 2016, **52**, 12614-12617.

8 J. Li, M. Yan, X. Zhou, Z.-Q. Huang, Z. Xia, C.-R. Chang, Y. Ma and Y. Qu, *Adv. Funct. Mater.*, 2016, **26**, 6785-6796.

9 S. She, Y. Zhu, H. A. Tahini, X. Wu, D. Guan, Y. Chen, J. Dai, Y. Chen, W. Tang, S. C Smith, H. Wang, W. Zhou and Z. Shao, *Small*, 2020, **16**, 2006800.

10 Y. Lu, Z. Li, Y. Xu, L. Tang, S. Xu, D. Li, J. Zhu and D. Jiang, *Chem. Eng. J.*, 2021, **411**, 128433.

11 Z. Cui, X. Liang, P. Wang, P. Zhou, Q. Zhang, Z. Wang, Z. Zheng, Y. Liu, Y. Dai and B. Huang, *Electrochim. Acta*, 2021, **395**, 139218.

12 Q. Chen, N. Gong, T. Zhu, C. Yang, W. Peng, Y. Li, F. Zhang and X. Fan, *Small*, 2022, **18**, 2105696.

13 C. Defilippi, D. V. Shinde, Z. Dang, L. Manna, C. Hardacre, A. J. Greer, C. D'Agostino and C. Giordano, *Angew. Chem. Int. Edit.*, 2019, **58**, 15464-15470.

14 A. Saad, Z. Cheng, X. Zhang, S. Liu, H. Shen, T. Thomas, J. Wang and M. Yang, *Adv. Mater. Interfaces*, 2019, **6**, 1900960.

15 S. H. Kwag, Y. S. Lee, J. Lee, D. I. Jeong, S. B. Kwon, J. H. Yoo, S. Woo, B. S. Lim, W. K. Park, M.-J. Kim, J. H. Kim, B. Lim, B. K. Kang, W. S. Yang and D. H. Yoon, *ACS Appl. Energy Mater.*, 2019, **2**, 8502-8510.

16 Y. Hu, D. Huang, J. Zhang, Y. Huang, M. S. J. T. Balogun and Y. Tong, *ChemCatChem*, 2019, **11**, 6051-6060.

17 Z. Yin, Y. Sun, C. Zhu, C. Li, X. Zhang and Y. Chen, *J. Mater. Chem. A*, 2017, **5**, 13648-13658.

18 G. Fu, Z. Cui, Y. Chen, L. Xu, Y. Tang and J. B. Goodenough, *Nano Energy*, 2017, **39**, 77-85.

19 C. Wu, X. Zhang, Z. Xia, M. Shu, H. Li, X. Xu, R. Si, A. I. Rykov, J. Wang, S. Yu, S. Wang and G. Sun, *J. Mater. Chem. A*, 2019, **7**, 14001-14010.

20 Z. Shao, J. Sun, N. Guo, F. He, K. Huang, F. Tian and Q. Wang, *J. Power Sources*, 2019, **422**, 33-41.

21 L. Zhu, B. Yang, Z. Wu, C. Li, H. Li, H. Li, Y. Huang, X. Zhu, X. Zhu and Y. Sun,

J. Mater. Sci. Technol., 2022, **112**, 222-229.

22 L. Yu, S. Song, B. McElhenny, F. Ding, D. Luo, Y. Yu, S. Chen and Z. Ren, *J. Mater. Chem. A*, 2019, **7**, 19728-19732.

23 X. Feng, H. Wang, X. Bo and L. Guo, *ACS Appl. Mater. Inter.*, 2019, **11**, 8018-8024.

24 L. Wang, Y. Li, X. Yin, Y. Wang, A. Song, X. Qin and G. Shao, *ACS Sustain. Chem. Eng.*, 2017, **5**, 7993-8003.

25 D. He, L. Cao, J. Huang, S. Li, Y. Feng, G. Li, F. Wang and L. Feng, *Chem. Eng. J.*, 2022, 429.

26 W. Wang, Y. Shao, Z. Wang, Z. Yang, Z. Zhen, Z. Zhang, C. Mao, X. Guo and G. Li, *ChemElectroChem*, 2020, 7, 1201-1206.

27 Y. Li, J. Zhang, X. Qian, Y. Zhang, Y. Wang, R. Hu, C. Yao and J. Zhu, *Appl. Surf. Sci.*, 2018, **427**, 884-889.

28 X. Xu, Y. Deng, M. Gu, B. Sun, Z. Liang, Y. Xue, Y. Guo, J. Tian and H. Cui, *Appl. Surf. Sci.*, 2019, **470**, 591-595.

29 N. Zhang, L. Cao, L. Feng, J. Huang, K. Kajiyoshi, C. Li, Q. Liu, D. Yang and J. He, *Nanoscale*, 2019, **11**, 11542-11549.